Carbon 145 (2019) 734–739

Contents lists available at ScienceDirect

Carbon

journal homepage: www.elsevier.com/locate/carbon

Colossal electric permittivity discovered in polyacrylonitrile (PAN) based carbon fiber, with comparison of PAN-based and pitch-based carbon fibers

Xiang Xi, D.D.L. Chung*

Composite Materials Research Laboratory, Department of Mechanical and Aerospace Engineering, University at Buffalo, The State University of New York, Buffalo, NY, 14260-4400, USA

ARTICLE INFO

Article history:
Received 28 September 2018
Received in revised form
14 January 2019
Accepted 20 January 2019
Available online 23 January 2019

ABSTRACT

The electric permittivity is a fundamental material property concerning the dielectric behavior. Colossal permittivity (relative permittivity exceeding 10,000) is attractive for capacitors, sensors, actuators and mechanical energy harvesters. It was discovered in this work in continuous polyacrylonitrile (PAN) based carbon fiber (Teijin's Tenax HTS45) along the fiber axis. This is the first report of colossal permittivity in carbon materials. The relative permittivity (12230 ± 990, 2 kHz) is much higher than that of mesophase-pitch-based carbon fiber (Cytec's Thornel P-25, 4384 ± 257, 2 kHz). The two fibers exhibit similar resistivity (1.52×10^{-3} and 1.24×10^{-3} Ω.cm for the PAN-based and pitch-based fibers, respectively). For both fibers, the permittivity is high, due to the physical continuity and mobile charge carriers. The higher permittivity of the PAN-based fiber compared to the pitch-based fiber is attributed to the higher degree of graphitization (as indicated by the lower interplanar spacing) of the PAN-based fiber. However, the smaller crystallite sizes and larger azimuthal spread of the carbon layers around the fiber axis cause the PAN-based fiber to be not higher in conductivity than the pitch-based fiber, in spite of the higher degree of graphitization. The smaller crystallite sizes and larger azimuthal spread are detrimental more to the conductivity than the polarization.

1. Introduction

Due to their electrical conductivity, carbon fibers are used in numerous electrical applications, such as susceptor induction heating, lightning protection, high-temperature conduction, and current collectors in batteries and supercapacitors. The polarization associated with the dielectric behavior gives an opposing electrical field, thus influencing the electrical conduction negatively. The capacitance also results in the RC time constant, thereby slowing down signal propagation. Thus, studying the dielectric behavior is necessary to support the electrical applications of carbon fibers.

The absorption/reflection of microwave or radio wave radiation (such as radiation in the GHz frequency range) by carbon materials has been researched by numerous workers for decades, particularly in relation to electromagnetic interference (EMI) shielding [1–6]. These carbon materials include continuous carbon fibers [7–10], due to their relevance to structural materials. However, the dielectric behavior at frequencies below the microwave, radio wave and optical ranges has received little attention, even though the low-frequency regime (which includes the utility frequencies, such as 60 Hz in the U.S.) is important for the abovementioned electrical applications. This paper addresses the dielectric behavior of continuous carbon fibers in the low-frequency regime.

The electrical permittivity is a fundamental material property that describes the dielectric behavior. Colossal permittivity refers to the behavior in which the relative permittivity is very high, typically exceeding 10,000. A high value of the relative permittivity is attractive for electrical energy storage in the form of a dielectric capacitor [11]. It also contributes to providing a high value of the piezoelectric coupling coefficient, as needed for piezoelectricity-based sensors, actuators and mechanical energy harvesters.

Colossal permittivity has been previously reported in ceramic oxides [12–21], such as those in the Perovskite family. These oxides exhibit high electrical resistivity, so they are attractive for functioning as the dielectric material in a dielectric capacitor. On the

* Corresponding author.
E-mail address: ddlchung@buffalo.edu (D.D.L. Chung).
URL: http://alum.mit.edu/www/ddlchung

https://doi.org/10.1016/j.carbon.2019.01.069
0008-6223/

other hand, for piezoelectricity-based mechanical energy harvesting, which involves converting mechanical energy to electrical energy using the direct piezoelectric effect, an intermediate level of electrical resistivity is needed. This is because the output electrical power is the product of the output voltage and the output current, so that both voltage and current need to be substantial. Resistivity that is too high will cause the output current to be small, whereas resistivity that is too low will cause the output voltage to be small. Ceramic and polymeric dielectric materials tend to exhibit high resistivity. Metals have recently been shown to exhibit colossal permittivity [22–24], but their resistivity is very low (ranging from 10^{-5} to 10^{-6} Ω.cm).

Carbon materials are attractively intermediate in the resistivity, which is typically of the order of 10^{-3} Ω.cm. The relative permittivity of carbon fibers have been shown to be high (3960 ± 450 and 4960 ± 662 at 2 kHz for Thornel P-25 and P-100 mesophase-pitch-based carbon fibers, respectively), though not colossal [25]. The relative permittivity of continuous unidirectional polyacrylonitrile (PAN) based carbon fiber polymer-matrix composite is also high (2160 ± 510 and 1640 ± 330 at 2 kHz for the longitudinal and transverse directions, respectively), though not colossal [26]. Based on these relative permittivity values of the composite and the fiber volume fraction, the relative permittivity of the fiber is obtained as 4352 ± 510 and 3310 ± 697 for the longitudinal and transverse directions, respectively [26]. Thus, carbon fibers have the potential of exhibiting the combination of high permittivity and intermediate resistivity that is needed for energy harvesting.

It is well-known that pitch-based carbon fibers are more ordered crystallographically than PAN-based carbon fibers fabricated at similar temperatures [27]. In other words, pitch is more graphitizable than PAN. The degree of order strongly affects the electrical, mechanical and other properties. In particular, the resistivity along the fiber axis decreases with increasing degree of order, partly due to the increase in the degree of preferred orientation of the carbon layers along the fiber axis as the degree of order increases. Comparison of the permittivity of the P-25 and P-100 fibers (with P-100 being more ordered than P-25) [25] suggests that a higher degree of order is associated with a higher permittivity. On the other hand, the permittivity and conductivity are not independent, according to the Kramers-Kronig Relationship [28]. Therefore, the reported difference in permittivity between the P-25 and P-100 fibers is at least partly due to the higher conductivity of P-100. In order to study the effect of the degree of order on the permittivity, fibers that exhibit similar resistivity values but different degrees of order should be investigated.

This paper is aimed at comparing the permittivity of pitch-based and PAN-based carbon fibers that exhibit similar values of the resistivity, thereby investigating the effect of the degree of order on the permittivity. In addition, due to the wide usage of PAN-based carbon fibers and the absence of prior work on the permittivity of PAN-based carbon fibers (to be distinguished from the PAN-based carbon fiber polymer-matrix composite of the prior work [26]), this paper is aimed at studying the permittivity of PAN-based carbon fiber. However, the finding of the paper has exceeded the aims, due to the unexpected discovery of colossal permittivity in the PAN-based carbon fiber.

2. Experimental methods

2.1. Materials

The continuous PAN-based carbon fiber is Teijin's Tenax-E HTS45 E23 12K 800tex, with 12,000 fibers per tow, fiber diameter 7.0 μm, density 1.77 g/cm^3, electrical resistivity 1.6×10^{-3} Ω.cm, tensile modulus 240 GPa, tensile strength 4500 MPa, and tensile ductility 1.9% [29,30]. The continuous mesophase-pitch-based carbon fiber is Cytec's Thornel P-25, with 2000 fibers per tow, fiber diameter 10 μm, density 1.92 g/cm^3, electrical resistivity 1.2×10^{-3} Ω.cm, tensile modulus 159 GPa, tensile strength 1560 MPa, and tensile ductility 0.9% [31]. The PAN-based fiber has lower density, higher modulus, higher strength, higher ductility, and slightly higher resistivity compared to the pitch-based fiber.

2.2. Permittivity measurement method

The method of permittivity measurement is an extension of the method of prior work for steels [22], aluminum [23], copper [24] and continuous carbon fiber polymer-matrix composite [26]. It involves a dielectric film between the specimen and each electrode (Fig. 1). The method also involves the decoupling of the interfacial capacitance from the volumetric capacitance, as explained below. In this context, the interface is that between the specimen and electrode, including the dielectric film. The specimen is a rectangular strip, with the long direction along the direction of capacitance measurement.

For decoupling the interfacial capacitance from the volumetric capacitance, four electrodes in the form of aluminum foil are positioned on the top surface of the specimen at four points (essentially equally spaced at a distance of ~76 mm, with the exact value measured for each specimen) along the length of the

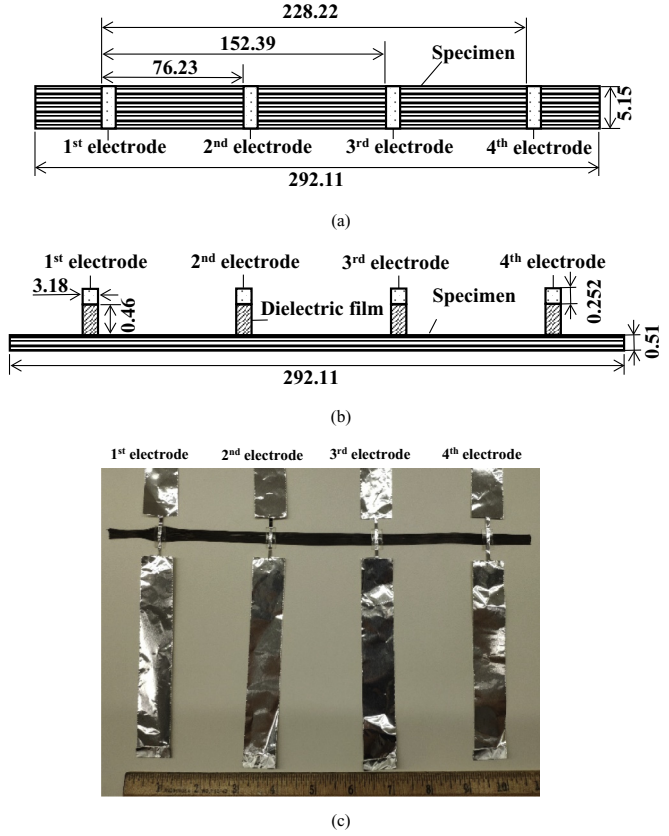

Fig. 1. Configuration for electric permittivity measurement. (a) Schematic illustration (top view), with the dimensions shown in mm for the PAN-based carbon fiber. (b) Schematic illustration (side view), with the dimensions shown in mm for the PAN-based carbon fiber, showing a dielectric film between each electrode and the specimen. The vertical axis is expanded, with the scale different from that of the horizontal axis. (c) Photograph of the PAN-based carbon fiber tow (horizontal) with four aluminum foil electrodes and including a ruler with main divisions in inches. Each electrode (3.18 mm wide) is much narrower for the region above the specimen than the regions away from the specimen.

specimen (Fig. 1). Each electrode is adhered to the top surface of the specimen by using 6 layers of double-sided adhesive tape (thickness 0.077 mm per layer, thickness 0.46 mm for the 6 layers combined), which serves as the dielectric film. Each electrode is 3.18 mm wide in the direction of the length of the specimen, such that it extends all the way along the 5.15 mm width of the specimen. By using different pairs of electrodes (the 1st and 2nd, the 1st and 3rd, and the 1st and 4th), measurement of the capacitance is conducted over distances of L (~76 mm), $2L$ (~152 mm) and $3L$ (~228 mm), with the exact values measured for each specimen.

The capacitance is measured using an LCR meter (Instek LCR-816 High Precision LCR Meter). The frequency is 2.000 kHz, because this is the highest frequency provided by the meter and a frequency in the kHz range is commonly available and widely used. The error in the capacitance measurement is ±0.0005 pF. The capacitance reported is that for the equivalent circuit of capacitance and resistance in series. This circuit model is intended to indicate the setting used in the meter, rather than the method of analysis. The voltage (0.300, 0.600 or 0.900 V) is adjusted so that the electric field (3.95 V/m) is the same for the different distances between the chosen electrodes of a pair.

The frequency for the capacitance measurement is fixed. In the case of discontinuous carbons (such as carbon black and activated carbon), prior work in this research group has shown that the permittivity decreases monotonically with increasing frequency from Hz to MHz [32–35].

The method of this work is in contrast to impedance spectroscopy [36–38], which involves measurement of the impedance (real and imaginary parts) as a function of the frequency and fitting the frequency dependence by using equivalent circuit models. Impedance spectroscopy suffers from the fact that the circuit models are not unique, so that the circuit parameters obtained by the curve fitting are not very meaningful scientifically.

For measurement using each pair of electrodes, the two interfacial capacitances (for the two specimen-electrode interfaces) and the specimen volumetric capacitance are three capacitors in series electrically. Hence, the measured capacitance C_m is given by

$$1/C_m = 1/C + 2/C_i, \tag{1}$$

Where C is the specimen volumetric capacitance, and C_i is the interfacial capacitance for one interface. The C relates to κ of the specimen by the equation

$$C = \varepsilon_o \kappa A/l, \tag{2}$$

Where ε_o is the permittivity of free space (8.85×10^{-12} F/m), A is the area of the specimen in the plane perpendicular to the direction of capacitance measurement, and l is the length of the specimen between the two electrodes in the direction of the capacitance measurement (i.e., L, $2L$ or $3L$). Combining Eqs. (1) and (2) gives

$$1/C_m = l/(\varepsilon_o \kappa A) + 2/C_i. \tag{3}$$

Based on Eq. (3), a plot of $1/C_m$ vs. l gives a line of slope equal to $1/(\varepsilon_o \kappa A)$. Hence, from the slope, κ is obtained.

2.3. Conductivity measurement method

The conductivity is measured using the same specimen configuration as Fig. 1, except that the dielectric film is replaced by silver paint. The same specimens are used first for permittivity measurement and then for conductivity measurement. By using different pairs of electrodes (the 1st and 2nd, the 1st and 3rd, and the 1st and 4th), measurement of the resistance is conducted over distances of L (~76 mm), $2L$ (~152 mm) and $3L$ (~228 mm), with the exact values measured for each specimen.

For measurement using each pair of electrodes, the two interfacial resistances and the specimen volumetric resistance are three resistors in series electrically. Hence, the measured resistance R_m is given by

$$R_m = R + 2R_i, \tag{4}$$

Where R is the specimen volumetric resistance, and R_i is the interfacial resistance for one interface. The R relates to the resistivity ρ of the specimen by the equation

$$R = \rho l/A, \tag{5}$$

Where A is the area of the specimen in the plane perpendicular to the direction of resistance measurement, and l is the length of the specimen between the two electrodes (i.e., L, $2L$ or $3L$).

Combining Eqs. (4) and (5) gives

$$R_m = \rho l/A + 2R_i, \tag{6}$$

Based on Eq. (6), a plot of R_m vs. l gives a line of slope equal to ρ/A. Hence, from the slope, ρ is obtained.

The DC resistance is measured using a precision digital multimeter (Keithley Model 2002) operating in the two-wire mode. For the range of resistance of this work, the resolution is 100 nΩ and the current provided by the meter is 7.2 mA [39].

3. Results and discussion

For both PAN-based and pitch-based carbon fibers, the plot of $1/C_m$ vs. distance l according to Eq. (1) and the plot of R_m vs. distance l according to Eq. (4) are highly linear. Figs. 2 and 3 give representative plots. The error in the relative permittivity κ or resistivity ρ is obtained by considering the range of values of the slope.

Table 1 shows that κ is much higher for the PAN-based carbon fiber than the pitch-based carbon fiber, while ρ is similar for the two types of fiber. The value for the pitch-based fiber (4383 ± 257) is close to the value (3960 ± 450, also at 2 kHz) previously reported for the same type of fiber (P-25), but using a different specimen testing set-up that involves using an alumina mold to hold multiple tows [25]. The resistivity value of $(1.52 \pm 0.04) \times 10^{-3}$ Ω.cm for the PAN-based carbon fiber is close to the manufacturer datasheet value of 1.6×10^{-3} Ω.cm [20]. The resistivity value of $(1.24 \pm 0.02) \times 10^{-3}$ Ω.cm for the pitch-based carbon fiber is close to the manufacturer datasheet value of 1.2×10^{-3} Ω.cm [31].

Since the resistivity is similar for the pitch-based carbon fiber (1.24×10^{-3} Ω.cm) and the PAN-based carbon fiber (1.52×10^{-3} Ω.cm), the huge difference in κ between these two fibers is attributed to the difference in structure between the two types of fiber, as discussed below.

The HTS PAN-based fiber of this work is very similar to the Hexcel AS-4 PAN-based carbon fiber in terms of the density (1.77 and 1.79 g/cm^3 for HTS and AS-4, respectively), fiber diameter (7.0 and 7.1 μm for HTS and AS-4, respectively), tensile modulus (240 GPa and 231 GPa for HTS and AS-4, respectively), tensile strength (4500 MPa and 4480 MPa for HTS and AS-4, respectively), tensile ductility (1.9% and 1.8% for HTS and AS-4, respectively) and electrical resistivity (1.6×10^{-3} and 1.7×10^{-3} Ω.cm, respectively). Due to the strong similarity in density and in mechanical and electrical properties between HTS and AS-4, these two PAN-based carbon fibers are considered to be essentially equivalent [40].

The L_c is 18 and 26 Å for AS-4 and P-25, respectively; L_a is 35 and 40 Å for AS-4 and P-25, respectively; the azimuthal spread is 36.8°

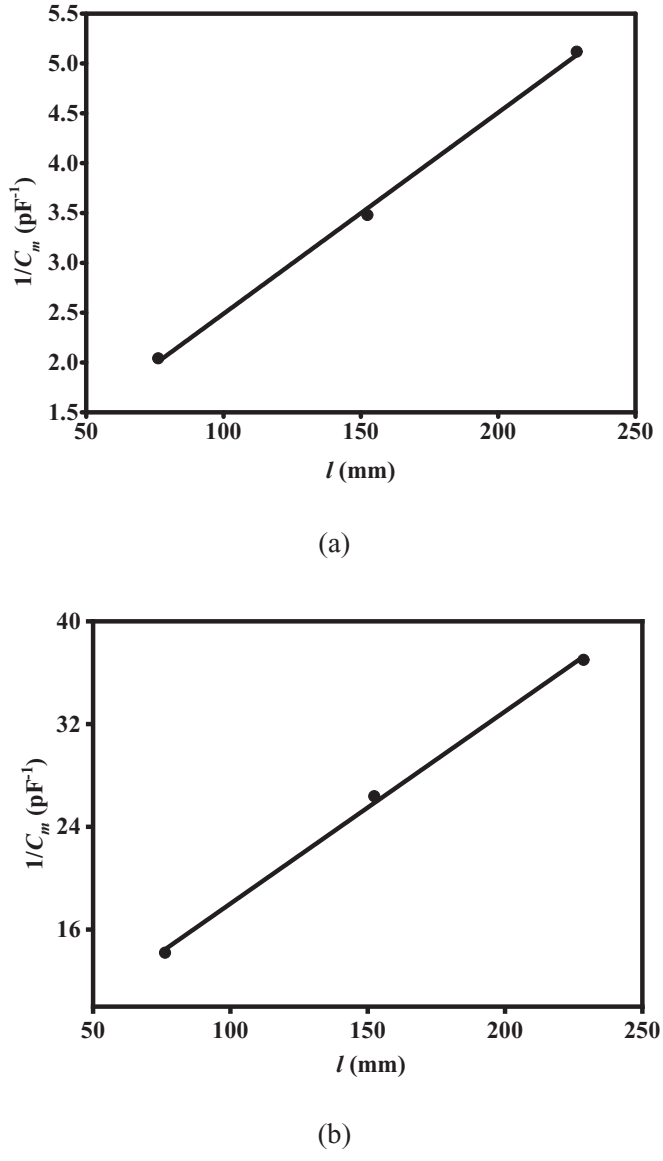

Fig. 2. Plot of $1/C_m$ vs. distance l according to Eq. (3). (a) PAN-based carbon fiber. (b) Pitch-based carbon fiber.

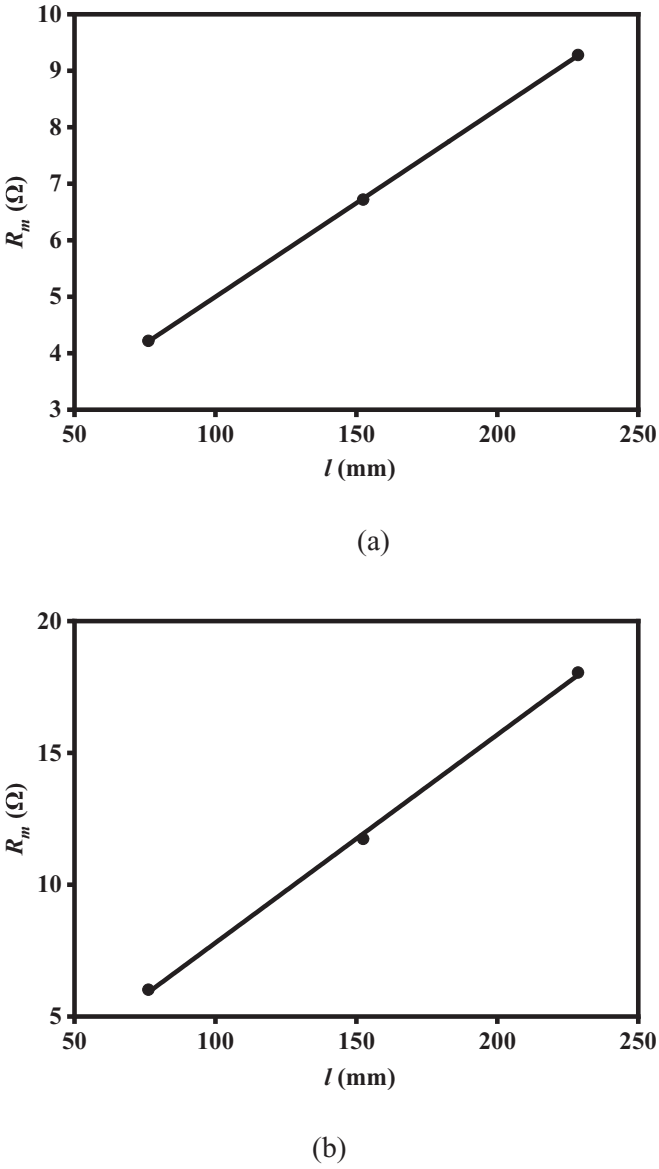

Fig. 3. Plot of R_m vs. distance l according to Eq. (6). (a) PAN-based carbon fiber. (b) Pitch-based carbon fiber.

and 31.9° for AS-4 and P-25, respectively [41]. On the other hand, the interplanar spacing d_{002} is 3.420 Å and 3.438 Å for AS-4 and P-25, respectively, corresponding to degree of graphitization of 0.24 and 0.02 for AS-4 and P-25, respectively [41]. Scanning electron microscopy of the fiber cross section shows the absence of observable layer-like microstructure for both AS-4 and P-25 [42], in contrast to the layer-like microstructure for P-100 [42], which is more graphitic. With the comparison between AS-4 and P-25 taken as a comparison between HTS and P-25, the above data indicate that HTS has lower L_c, lower L_a, larger azimuthal spread and, most significantly, lower d_{002} than P-25.

With HTS (PAN-based) exhibiting higher permittivity than P-25 (pitch-based) (Table 1), the above arguments mean that the axial permittivity of carbon fiber is enhanced by a higher degree of graphitization, as indicated by a lower d_{002}. On the other hand, HTS and P-25 exhibit about the same conductivity (Table 1). This is due to the PAN-based fiber's lower degree of carbon layer preferred orientation and smaller crystallite size, which cause the higher degree of graphitization alone to be not able to cause the PAN-based fiber to be more conductive than the pitch-based fiber. The permittivity is less sensitive to interfaces than the DC conductivity, due to the smaller distance of excursion for the charge carriers during AC polarization than during DC conduction. As a consequence, the greater number of interfaces in the PAN-based fiber, as caused by the smaller crystallite size and lower degree of preferred orientation, does not decrease the permittivity of the PAN-based fiber as much as decreasing its conductivity. Therefore, the two types of fiber exhibit essentially the same conductivity, while the permittivity is higher for the PAN-based fiber than the

Table 1
Relative permittivity (2 kHz) and electrical resistivity (DC) of PAN-based and pitch-based carbon fibers.

	PAN-based carbon fiber	Pitch-based carbon fiber
Relative permittivity	12233 ± 994	4384 ± 257
Resistivity (10^{-3} Ω.cm)	1.52 ± 0.04	1.24 ± 0.02

pitch-based fiber. Investigation of a larger variety of carbon fibers is needed to ascertain the relationship between the permittivity and the fiber structure.

The finding that, for the same conductivity, less microstructural order promotes the permittivity is consistent with the following additional notions. Firstly, less microstructural order increases the number of carbon layers that are not along the fiber axis and these carbon layers contribute to the axial permittivity of the fiber more than the carbon layers that are oriented along the fiber axis (due to the parallel-plate capacitor geometry of the parallel carbon layers). Secondly, less microstructural order decreases L_c and L_a, thereby increasing the number of carbon layer stacks and, as a consequence, increasing the number of inter-stack interfaces, which contribute to the capacitance.

Prior work of this research groups has shown that the relative permittivity is 4960 ± 662 and 3960 ± 450 for Thornel P-100 (more graphitic) and Thornel P-25 fibers (less graphitic), respectively [25]. The higher permittivity of P-100 compared to P-25 is attributed to the much lower resistivity of P-100 (1.8×10^{-4} Ω.cm compared to 1.2×10^{-3} Ω.cm for P-25) and the fact that the permittivity and conductivity are not independent of one another. More charge carrier movement, as enabled by a lower resistivity, promotes polarization, thereby increasing the permittivity.

The relative permittivity values of all the continuous carbon fibers mentioned above are higher than those of discontinuous carbons (such as carbon black, exfoliated graphite, natural graphite, activated carbon, graphite oxide and reduced graphite oxide) that have been tested by this research group [32–35]. The relatively low values for the discontinuous carbons are due to the small dimensions of the discontinuous carbons and the resulting limited distance of excursion of the charge carriers during polarization.

The nickel coating of the carbon fiber greatly increases the permittivity, as shown in our parallel study [43]. The effect of defects on the permittivity of carbon fiber is yet to be studied.

The permittivity of the carbon electrodes in electrochemical devices (supercapacitors and batteries) is expected to affect the device performance. In particular, the polarization of the electrode results in an opposing electric field, which can affect the device performance negatively. The polarization is particularly significant under DC operation, which is the case for batteries. Furthermore, the RC time constant resulting from the capacitance of the electrode may degrade the ability of the device to operate at high frequencies. The practically important effects of the electrode polarization have been neglected in prior research on the electrochemical devices, but they are worthy of future research.

4. Conclusion

Colossal permittivity was discovered in PAN-based carbon fiber along the fiber axis. This is the first report of colossal permittivity in carbon materials. The relative permittivity (12233 ± 994 at 2 kHz) is much higher than that of mesophase-pitch-based carbon fiber (4384 ± 257 at 2 kHz). The two types of fiber exhibit similar resistivity (1.52×10^{-3} and 1.24×10^{-3} Ω.cm for the PAN-based and pitch-based fibers, respectively). For both types of carbon fiber, the relative permittivity is high, due to the material continuity and mobile charge carriers of the fiber. The colossal permittivity of the PAN-based carbon fiber is attributed to the high degree of graphitization (as indicated by the small interplanar spacing) of the PAN-based carbon fiber compared to the pitch-based carbon fiber. On the other hand, the lower degree of microstructural order (as indicated by lower L_c, lower L_a and larger azimuthal spread) of the PAN-based fiber compared to the pitch-based fiber causes the conductivity to be not higher for the PAN-based fiber, in spite of the higher degree of graphitization of the PAN-based fiber. The conduction is more sensitive to the microstructural order than the polarization. As a consequence, the PAN-based fiber exhibits higher permittivity than the pitch-based fiber, while the two fibers are similar in the conductivity.

The combination of colossal permittivity and intermediate conductivity of the PAN-based carbon fiber is in contrast to the colossal permittivity and low conductivity of previously reported ceramics [2–11]. The intermediate conductivity is attractive for enhancing the output electric power in mechanical energy harvesting. The piezoelectric behavior of the PAN-based carbon fiber is the subject of a separate paper [44].

References

[1] Y. Jia, K. Li, L. Xue, J. Ren, S. Zhang, H. Li, Mechanical and electromagnetic shielding performance of carbon fiber reinforced multilayered (PyC-SiC)n matrix composites, Carbon 111 (2017) 299–308.

[2] M. Hong, W. Choi, K. An, S. Kang, S. Park, Y. Lee, B. Kim, Electromagnetic interference shielding behaviors of carbon fibers-reinforced polypropylene matrix composites: II. Effects of filler length control, J. Ind. Eng. Chem. (Amsterdam, Netherlands) 20 (5) (2014) 3901–3904.

[3] S. Gong, Z.H. Zhu, M. Arjmand, U. Sundararaj, J.T.W. Yeow, W. Zheng, Effect of carbon nanotubes on electromagnetic interference shielding of carbon fiber reinforced polymer composites, Polym. Compos. 39 (S2) (2018) E655–E663.

[4] M. Cao, W. Song, Z. Hou, B. Wen, J. Yuan, The effects of temperature and frequency on the dielectric properties, electromagnetic interference shielding and microwave-absorption of short carbon fiber/silica composites, Carbon 48 (3) (2010) 788–796.

[5] D.D.L. Chung, Carbon materials for structural self-sensing, electromagnetic shielding and thermal interfacing, Carbon 50 (2012) 3342–3353.

[6] J. Wu, Z. Ye, H. Ge, J. Chen, W. Liu, Z. Liu, Modified carbon fiber/magnetic graphene/epoxy composites with synergistic effect for electromagnetic interference shielding over broad frequency band, J. Colloid Interface Sci. 506 (2017) 217–226.

[7] D.D.L. Chung, A.A. Eddib, Effect of fiber lay-up configuration on the electromagnetic interference shielding effectiveness of continuous carbon fiber polymer-matrix composite, Carbon 141 (2019) 685–691.

[8] A.A. Eddib, D.D.L. Chung, Radio-frequency linear absorption coefficient of carbon materials, its dependence on the thickness and its independence on the carbon structure, Carbon 124 (2017) 473–478.

[9] D. Micheli, S. Laurenzi, P.V. Mariani, F. Moglie, G. Gradoni, M. Marchetti, Electromagnetic Shielding of Oriented Carbon Fiber Composite Materials. European Space Agency, Proc ESA Workshop on Aerospace EMC, 2012 a3/1-a3/5, [Special Publication] SP 2012;SP-702.

[10] X. Luo, D.D.L. Chung, Electromagnetic interference shielding using continuous carbon fiber carbon-matrix and polymer-matrix composites, Composites Part B 30 (3) (1999) 227–231.

[11] D.D.L. Chung, Development, design and applications of structural capacitors, Appl. Energy 231 (2018) 89–101.

[12] Z. Liu, C. Zhao, B. Wu, J. Wu, Reduced dielectric loss in new colossal permittivity (Pr, Nb)TiO_2 ceramics by suppressing adverse effects of secondary phases, Phys. Chem. Chem. Phys. 20 (34) (2018) 21814–21821.

[13] B. Guo, P. Liu, X. Cui, Y. Song, Colossal permittivity and dielectric relaxations in $(La_{0.5}Nb_{0.5})_xTi_{1-x}O_2$ ceramics, J. Alloy. Comp. 768 (2018) 368–376.

[14] K. Liu, Y. Sun, F. Zheng, M. Tse, Q. Sun, Y. Liu, J. Hao, A general strategy to achieve colossal permittivity and low dielectric loss through constructing insulator/semiconductor/insulator multilayer structures, J. Low Temp. Phys. 192 (5–6) (2018) 346–358.

[15] Z. Wang, H. Chen, T. Wang, Y. Xiao, W. Nian, J. Fan, Enhanced relative permittivity in niobium and europium co-doped TiO_2 ceramics, J. Eur. Ceram. Soc. 38 (11) (2018) 3847–3852.

[16] Y. Wu, J. Li, H. Bai, S. He, Y. Hong, K. Shi, Zhou, Colossal dielectric behavior and dielectric relaxation of (Li, Fe) co-doped ZnO ceramics, Phys. Status Solidi RRL: Rapid Res. Lett. 12 (6) (2018) (NA).

[17] S. De Almeida-Didry, M.M. Nomel, C. Autret, C. Honstettre, A. Lucas, F. Pacreau, F. Gervais, Control of grain boundary in alumina doped CCTO showing colossal permittivity by core-shell approach, J. Eur. Ceram. Soc. 38 (9) (2018) 3182–3187.

[18] X.W. Wang, B.H. Zhang, L.Y. Sun, W.N. Qiao, Y.D. Hao, Y.C. Hu, X.E. Wang, Colossal dielectric properties in $(Ta_{0.5}Al_{0.5})_xTi_{1-x}O_2$ ceramics, J. Alloy. Comp. 745 (2018) 856–862.

[19] L. Li, T. Lu, N. Zhang, J. Li, Z. Cai, The effect of segregation structure on the colossal permittivity properties of $(La_{0.5}Nb_{0.5})_xTi_{1-x}O_2$ ceramics, J. Mater. Chem. C 6 (9) (2018) 2283–2294.

[20] C. Zhao, J. Wu, Effects of secondary phases on the high-performance colossal permittivity in titanium dioxide ceramics, ACS Appl. Mater. Interfaces 10 (4) (2018) 3680–3688.

[21] Y. Yu, W. Li, Y. Zhao, T. Zhang, R. Song, Y. Zhang, Z. Wang, W. Fei, Large-size-mismatch co-dopants for colossal permittivity rutile TiO_2 ceramics with temperature stability, J. Eur. Ceram. Soc. 38 (4) (2018) 1576–1582.

[22] D.D.L. Chung, K. Shi, Sensing the stress in steel by capacitance measurement, Sensor. Actuator. 274 (2018) 244–251.
[23] X. Xi, D.D.L. Chung, Capacitance-based nondestructive evaluation of aluminum, with measurement of the electric permittivity, submitted.
[24] X Xi, D.D.L. Chung, Electric permittivity of copper and its dependence on stress and surface oxidation, submitted.
[25] A.A. Eddib, D.D.L. Chung, Electric permittivity of carbon fiber, Carbon 143 (2019) 475–480.
[26] A.A. Eddib, D.D.L. Chung, First report of capacitance-based self-sensing and in-plane electric permittivity of carbon fiber polymer-matrix composite, Carbon 140 (2018) 413–427.
[27] D.D.L. Chung, Carbon Materials, World Scientific, Singapore, 2018. Ch. 6.
[28] https://en.wikipedia.org/wiki/Kramers%E2%80%93Kronig_relations (as viewed on Sept. 7, 2018).
[29] http://ase.au.dk/fileadmin/www.ase.au.dk/Filer/Laboratorier_og_vaerksteder/Komposit-lab/Fiber/Carbon/Carbon_UD_HS__194_gsm__Tenax-E_HTS45_E23_-_TDS.pdf (as viewed on Sept. 22, 2018).
[30] http://pdf.directindustry.com/pdf/toho-tenax-europe-gmbh/tenax-e-hts45-p12-12k/37818-629937.html (as viewed on Sept.22, 2018).
[31] https://cytec.com/sites/default/files/datasheets/THORNEL_P25_052112.pdf (as viewed on Sept. 22, 2018).
[32] A. Wang, D.D.L. Chung, Dielectric and electrical conduction behavior of carbon paste electrochemical electrodes, with decoupling of carbon, electrolyte and interface contributions, Carbon 72 (2014) 135–151.
[33] X. Hong, D.D.L. Chung, Exfoliated graphite with relative dielectric constant reaching 360, obtained by exfoliation of acid-intercalated graphite flakes without subsequent removal of the residual acidity, Carbon 91 (2015) 1–10.
[34] X. Hong, W. Yu, A. Wang, D.D.L. Chung, Graphite oxide paper as a polarizable electrical conductor in the through-thickness direction, Carbon 109 (2016) 874–882.
[35] X. Hong, W. Yu, D.D.L. Chung, Electric permittivity of reduced graphite oxide, Carbon 111 (2017) 182–190.
[36] E. Sentuerk, M. Okutan, S.E. San, O. Koeysal, Debye type dielectric relaxation in carbon nano-balls' and 4-DMAABCA acid doped E7 coded nematic liquid crystal, J. Non-Cryst. Solids 354 (30) (2008) 3525–3528.
[37] P. Xie, W. Sun, Y. Liu, A. Du, Z. Zhang, G. Wu, R. Fan, Carbon aerogels towards new candidates for double negative metamaterials of low density, Carbon 129 (2018) 598–606.
[38] P. Xie, Z. Zhang, K. Liu, L. Qian, F. Dang, Y. Liu, R. Fan, X. Wang, S. Dou, C/SiO2 meta-composite: overcoming the λ/a relationship limitation in metamaterials, Carbon 125 (2017) 1–8.
[39] https://xdevs.com/doc/Keithley/2002/SPEC-2002.pdf (as viewed on Sept. 22, 2018).
[40] Teijin Carbon America, Inc., Private Communication.
[41] D.P. Anderson, Carbon Fiber Morphology, II: Expanded Wide-Angle X-Ray Diffraction Studies of Carbon Fibers. AD-A235 599, WRDC-TR-90-4137, Interim Report for Period Dec. 1988 – April 1990. Wright Laboratory, Air Force Systems Command, Wright-Patterson Air Force, Ohio, 1991 as viewed on Sept. 27, 2018, http://www.dtic.mil/dtic/tr/fulltext/u2/a235599.pdf.
[42] J.B. Ferguson, D.P. Anderson, K.L. Strong, Thermoelectric properties of carbon fibers, in: Thermal Conductivity 30, Thermal Expansion 18, Joint Conferences, August 29 - September 2, 2009, pp. 768–773. Pittsburgh, Pennsylvania, USA.
[43] X. Xi, D.D.L. Chung, Effect of nickel coating on the stress-dependent electric permittivity, piezoelectricity and piezoresistivity of carbon fiber, with relevance to stress self-sensing, Carbon 145 (2019) 401–410.
[44] X. Xi, D.D.L. Chung, Piezoelectric and piezoresistive behavior of unmodified carbon fiber, Carbon 145 (2019) 452–461.